PHYSICAL REVIEW D **90,** 091701(R) (2014)

Limits on light weakly interacting massive particles from the CDEX-1 experiment with a *p*-type point-contact germanium detector at the China Jinping Underground Laboratory

Q. Yue,[1,*] W. Zhao,[1,†] K. J. Kang,[1] J. P. Cheng,[1] Y. J. Li,[1] S. T. Lin,[2,7,‡] J. P. Chang,[5] N. Chen,[1] Q. H. Chen,[1] Y. H. Chen,[6] Y. C. Chuang,[7,§] Z. Deng,[1] Q. Du,[4] H. Gong,[1] X. Q. Hao,[1] H. J. He,[1] Q. J. He,[1] H. X. Huang,[3] T. R. Huang,[7,§] H. Jiang,[1] H. B. Li,[7,§] J. M. Li,[1] J. Li,[1] J. Li,[5] X. Li,[3] X. Y. Li,[4] Y. L. Li,[1] H. Y. Liao,[7,§] F. K. Lin,[7,§] S. K. Liu,[2] L. C. Lü,[1] H. Ma,[1] S. J. Mao,[5] J. Q. Qin,[1] J. Ren,[3] J. Ren,[1] X. C. Ruan,[3] M. B. Shen,[6] L. Singh,[7,8,§] M. K. Singh,[7,8,§] A. K. Soma,[7,§] J. Su,[1] C. J. Tang,[2] C. H. Tseng,[7,§] J. M. Wang,[6] L. Wang,[1] Q. Wang,[1] H. T. Wong,[7,§] S. Y. Wu,[6] Y. C. Wu,[1] Y. C. Wu,[5] Z. Z. Xianyu,[1] R. Q. Xiao,[1] H. Y. Xing,[2] F. Z. Xu,[1] Y. Xu,[4] X. J. Xu,[1] T. Xue,[1] L. T. Yang,[1] S. W. Yang,[7,§] N. Yi,[1] C. X. Yu,[4] H. Yu,[1] X. Z. Yu,[2] X. H. Zeng,[6] Z. Zeng,[1] L. Zhang,[5] Y. H. Zhang,[6] M. G. Zhao,[4] Z. Y. Zhou,[3] J. J. Zhu,[2] W. B. Zhu,[5] X. Z. Zhu,[1] Z. H. Zhu[6]

(CDEX Collaboration)

[1]*Key Laboratory of Particle and Radiation Imaging (Ministry of Education) and Department of Engineering Physics, Tsinghua University, Beijing 100084*
[2]*College of Physical Science and Technology, Sichuan University, Chengdu 610064*
[3]*Department of Nuclear Physics, China Institute of Atomic Energy, Beijing 102413*
[4]*School of Physics, Nankai University, Tianjin 300071*
[5]*NUCTECH Company, Beijing 10084*
[6]*YaLong River Hydropower Development Company, Chengdu 610051*
[7]*Institute of Physics, Academia Sinica, Taipei 11529*
[8]*Department of Physics, Banaras Hindu University, Varanasi 221005*

(Received 22 April 2014; revised manuscript received 8 September 2014; published 10 November 2014)

We report results of a search for light dark matter weakly interacting massive particles (WIMPs) with CDEX-1 experiment at the China Jinping Underground Laboratory, based on 53.9 kg-days of data from a *p*-type point-contact germanium detector enclosed by a NaI(Tl) crystal scintillator as anti-Compton detector. The event rate and spectrum above the analysis threshold of 475 eVee are consistent with the understood background model. Part of the allowed regions for WIMP-nucleus coherent elastic scattering at WIMP mass of 6–20 GeV are probed and excluded. Independent of interaction channels, this result contradicts the interpretation that the anomalous excesses of the CoGeNT experiment are induced by dark matter, since identical detector techniques are used in both experiments.

DOI: 10.1103/PhysRevD.90.091701 PACS numbers: 95.35.+d, 29.40.-n, 95.55.Vj

Current direct-detection dark matter experiments aim at searching of the weakly interacting massive particles (WIMPs, denoted by χ) via elastic scattering of nuclei in terrestrial detectors: $\chi + N \to \chi + N$ [1]. Of particular interest are the potential positive signatures implied by data from the DAMA [2], CoGeNT [3], CRESST-II [4] and CDMS-II(Si) [5] experiments. Such interpretations, however, are in conflict with the null results from other experiments [6–10]. Additional experiments with improved sensitivities to probe this parameter space are crucial.

Germanium detectors with sub-keV sensitivities were identified [11] as effective means to probe the light WIMP regions, motivating development of *p*-type point-contact germanium detectors (*p*PCGe) [12] and various experimental searches [3,8,13–15]. In particular, the CoGeNT experiment [3] with a 443 g *p*PCGe detector reported possible WIMP-induced events as well as annual modulation signatures.

The China Dark Matter Experiment (CDEX) pursues direct searches of light WIMPs towards the goal of a ton-scale germanium detector array at the China Jinping Underground Laboratory (CJPL) [16,17] located in Sichuan, China, with about 2400 m of rock overburden. The combined cosmic-ray direct and induced rates at CJPL have been measured [17] to be 61.7 $m^{-2}\,yr^{-1}$, consistent with expectations. Studies from a prototype CDEX-0 detector array with 20 g target mass at CJPL were reported [18]. Our earlier measurement at CJPL from the first phase of CDEX experiment (CDEX-1) [14] is with a *p*PCGe of target mass 994 g and analysis threshold of 400 eVee ("ee" denotes electron-equivalent energy), but in the absence of anti-Compton (AC) detector and prior to surface event

*Corresponding author.
yueq@mail.tsinghua.edu.cn
†Corresponding author.
w-zhao11@mail.tsinghua.edu.cn
‡Corresponding author.
linst@phys.sinica.edu.tw
§Participating as a member of TEXONO Collaboration.

suppression. We report new CDEX-1 results in this article with these two crucial features incorporated. A cylindrical NaI(Tl) crystal scintillator with a well-shaped cavity enclosing the *p*PCGe target serves as the AC detector. Identification of surface background and derivation of efficiency factors follow the procedures of Ref. [19]. Details of the hardware setup and shielding configurations can be referred to Refs. [14,20].

Signals from the p^+ point-contact electrode are processed by a pulsed reset preamplifier with three identical outputs. Two of them are distributed to the shaping amplifiers at 12 μs and 6 μs shaping time which also provides the trigger for data acquisition (DAQ), as well as the energy measurement (T). The remaining one is loaded to a timing amplifier (TA) which provides the fast rise-time information. The outputs are digitized by flash analog-to-digital converters at 100 MHz. A total of 58.7 days of data was recorded at a trigger rate of ~5 Hz. The DAQ dead time is 0.1%, as measured by events due to random triggers (RT) generated by a precision pulser. Energy calibration was achieved by the cosmogenic x-ray peaks and the zero-energy was defined by the pedestals of RT events. Deviations from linearity is less than 0.8%. The trigger efficiency was unity above 320 eVee, as verified by *in situ* physics events via an extrapolation of the amplitude distributions to subnoise edge energy [13]. The selection of candidate events based on timing correlation and basic pulse shape discrimination ("Basic Cut," denoted by BC) as well as the derivation of their efficiencies were discussed in our earlier report [14]. The microphonics effects and electronic events induced by the preamplifier reset timing were completely suppressed and the combined efficiencies of 86.3% were accurately evaluated. Events in anticoincidence (coincidence) with the AC detector are denoted by $\mathrm{AC}^-(^+)$. The AC^- selection discriminate γ-ray induced background at a signal efficiency of ~100%, as measured by RT events.

The n^+ surface electrode of *p*PCGe is fabricated by diffusion of lithium ions, having a finite thickness and producing events with anomalous charge collection and rise time (τ) [19,21]. The thickness of the surface layer, including both the dead and inactive layers, was derived to be (0.97 ± 0.15) mm, via the comparison of measured and simulated intensity ratios of various γ peaks from a ^{133}Ba source, with the thickness of the copper cryostat being the leading contribution to the uncertainties [22]. This gives rise to a fiducial mass of 919 g and data strength of 53.9 kg-days for this analysis. Surface events have anomalous charge collection and rise-time (τ) distributions. The τ values are measured by fitting to a hyperbolic tangent function to the TA signals [19]. The τ distribution of AC^- events is depicted in Fig. 1(a), showing the two-band structure characterizing bulk (B) and surface (S) events. Typical B and S events at 500 eVee, together with their fitted profiles, are displayed in the inset. The τ distributions

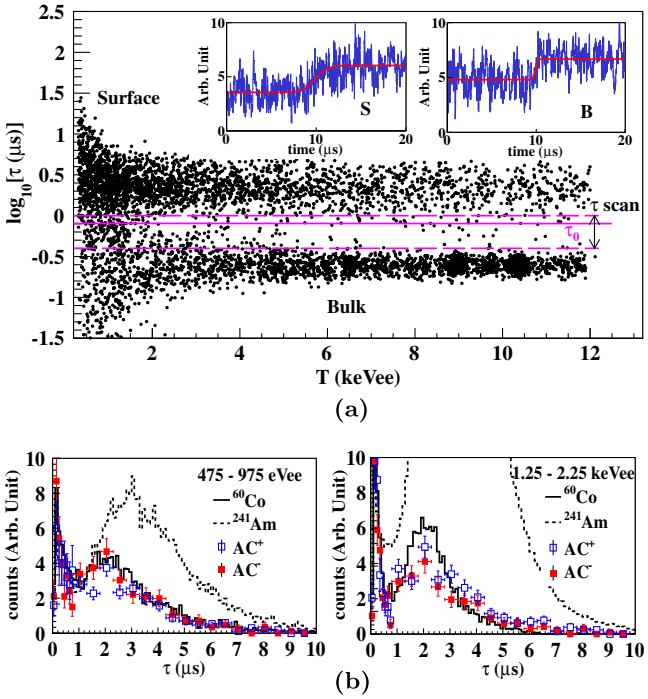

FIG. 1 (color online). (a) Scatter plot of the *p*PCGe rise time ($\log_{10}[\tau]$) versus deposited energy for AC^- events. The τ_0 line corresponds to the BS cut in this analysis, with dashed lines indicating the range of cut-stability test. Typical B(S) pulses at energy of ~500 eVee are depicted in the insets. (b) τ distributions with ^{241}Am and ^{60}Co γ sources, together with that from AC^+ and AC^- background data after BS cut, in the two energy bins of 475–975 eVee (left) and 1.25–2.25 keVee (right).

of AC^- and AC^+ events at two energy bands are depicted in of Fig. 1(b), together with those from ^{60}Co γ source. The three samples match well, indicating that the *in situ* background is dominated by ambient high energy (MeV range) γ's. Events due to low energy γ's from ^{241}Am γ source, also superimposed, show differences in the τ distributions in S.

The τ cut(τ_0) for differentiating the observed B and S events is set at 0.8 μs. Two factors are necessary to translate the measured rates (B,S) to the actual rates $(\mathrm{B}_0, \mathrm{S}_0)$—the B-signal retaining ($\varepsilon_{\mathrm{BS}}$) and S-background rejection (λ_{BS}) efficiencies. These are related by the coupled equations:

$$\begin{aligned} \mathrm{B} &= \varepsilon_{\mathrm{BS}} \cdot \mathrm{B}_0 + (1 - \lambda_{\mathrm{BS}}) \cdot \mathrm{S}_0 \\ \mathrm{S} &= (1 - \varepsilon_{\mathrm{BS}}) \cdot \mathrm{B}_0 + \lambda_{\mathrm{BS}} \cdot \mathrm{S}_0. \end{aligned} \quad (1)$$

The normalization of $(\mathrm{B}_0, \mathrm{S}_0) = (\mathrm{B}, \mathrm{S})$ is set at the high energy range of 3–5 keVee where the separation of the two bands is larger than the τ-measurement resolution.

Calibration data with ^{241}Am, ^{57}Co, ^{137}Cs and ^{60}Co are adopted to evaluate $(\varepsilon_{\mathrm{BS}}, \lambda_{\mathrm{BS}})$. Figure 2(a) shows the measured B spectra and their corresponding reference B_0 derived from simulation. The allowed bands in $(\varepsilon_{\mathrm{BS}}, \lambda_{\mathrm{BS}})$ derived from the calibration data at 475–575 eVee and

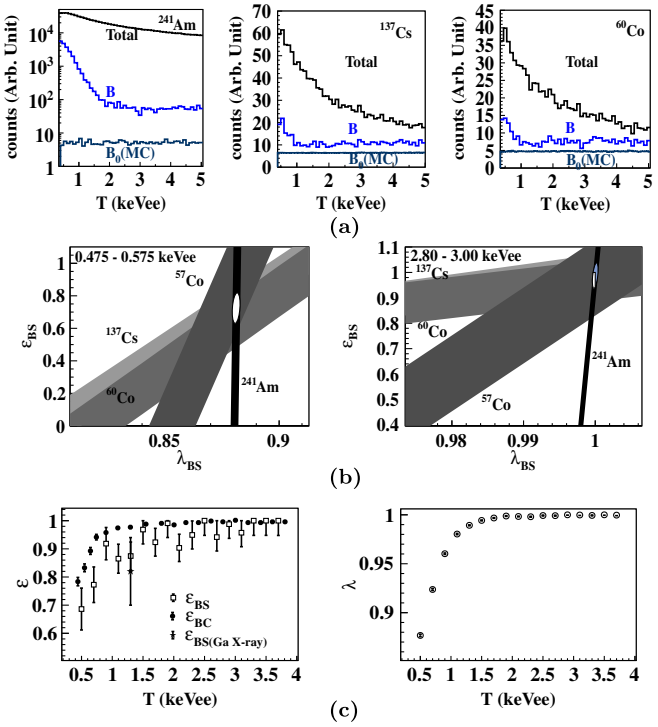

FIG. 2 (color online). Derivation of $(\epsilon_{\rm BS}, \lambda_{\rm BS})$ with ^{241}Am, ^{60}Co, ^{137}Cs and ^{60}Co sources. (a) The measured Total and B spectra, in comparison with B_0 from simulations. (b) Allowed bands at 475–575 eVee and at 2.8–3.0 keVee. (c) The measured $(\epsilon_{\rm BS}, \lambda_{\rm BS})$ and $\epsilon_{\rm BC}$ as functions of energy. Independent measurement on $\epsilon_{\rm BS}$ with Ga-L x rays is included.

2.8–3.0 keVee are illustrated in Fig. 2(b). The bands overlap at a common region indicating the results are valid over the entire energy range of interest. The measured $(\epsilon_{\rm BS}, \lambda_{\rm BS})$ as a function of energy are depicted in Fig. 2(c). An additional consistency measurement is provided by the ratio of the Ga-L x rays at 1.3 keVee after τ selection to its original intensity predicted by the Ga-K x ray at 10.37 keVee.

The raw spectrum and those at various stages of selection procedures are depicted in Fig. 3(a). The peak at 600 eVee is due to induced electronic noise from preamplifier resets and is completely rejected by timing correlation in BC [14]. The $(\epsilon_{\rm BS}, \lambda_{\rm BS})$-corrected spectra of the candidate events, defined as $\mathrm{AC}^- \otimes \mathrm{B}_0$ and shown in the Fig. 3(b), can be derived via the solution of Eq. (1):

$$\mathrm{B}_0 = \frac{\lambda_{\rm BS}}{\epsilon_{\rm BS}+\lambda_{\rm BS}-1}\cdot \mathrm{B} + \frac{\lambda_{\rm BS}-1}{\epsilon_{\rm BS}+\lambda_{\rm BS}-1}\cdot \mathrm{S}$$
$$\mathrm{S}_0 = \frac{\epsilon_{\rm BS}-1}{\epsilon_{\rm BS}+\lambda_{\rm BS}-1}\cdot \mathrm{B} + \frac{\epsilon_{\rm BS}}{\epsilon_{\rm BS}+\lambda_{\rm BS}-1}\cdot \mathrm{S}. \qquad (2)$$

The peaks correspond to known K-shell x rays from the cosmogenically activated isotopes. The analysis threshold is placed at 475 eVee, below which the sensitivity is

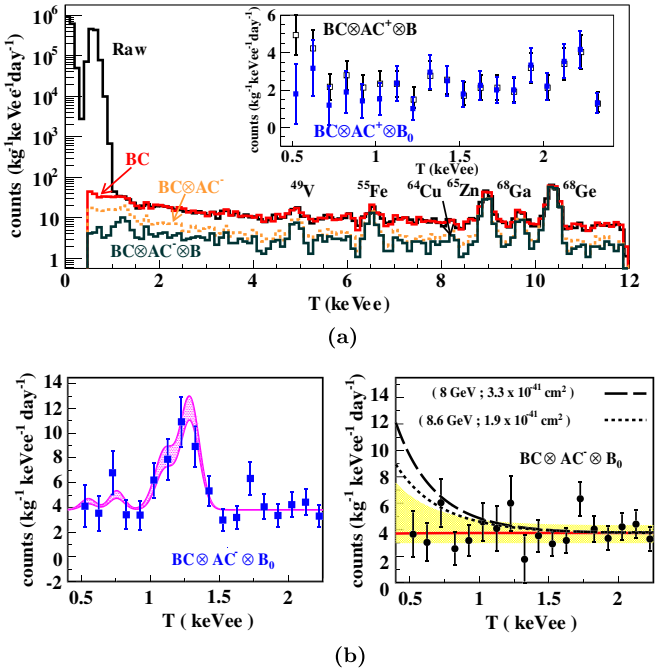

FIG. 3 (color online). (a) Measured energy spectra, showing the raw data with those at various stages of the selection procedures including the BC and AC and BS cuts. The inset shows the B spectra of AC^+, before and after $(\epsilon_{\rm BS}, \lambda_{\rm BS})$ correction. (b) The $(\epsilon_{\rm BS}, \lambda_{\rm BS})$-corrected $\mathrm{BC} \otimes \mathrm{AC}^- \otimes \mathrm{B}_0$ spectrum—Left: The L-X lines predicted by the K-X intensities. Right: Residual with the L-X peaks subtracted, together with the best-fit profile and 2σ uncertainty band at $\mathrm{m}_\chi = 8$ GeV, as well as recoil spectra at the best-fit values of CoGeNT-2013 [3] and CDMS(Si) [5] at $(\mathrm{m}_\chi; \sigma^{\rm SI}_{\chi \rm N}) = (8\ \mathrm{GeV}; 3.3\times10^{-41}\ \mathrm{cm}^2)$ and $(8.6\ \mathrm{GeV}; 1.9\times10^{-41}\ \mathrm{cm}^2)$, respectively.

constrained by the noise edge. The AC^+ spectra, depicted in the inset of Fig 3(a), correspond to events from ambient γ rays which are in coincidence with the NaI(Tl) detector. An expected flat $\mathrm{AC}^+ \otimes \mathrm{B}_0$ spectrum down to threshold is obtained, demonstrating that the $(\epsilon_{\rm BS}, \lambda_{\rm BS})$ correction is valid.

The various components which contribute to the errors of $\mathrm{AC}^- \otimes \mathrm{B}_0$ at threshold and at a typical high energy bin are summarized in Table I. Uncertainty values of $(\epsilon_{\rm BS}, \lambda_{\rm BS})$ and B_0 at threshold are listed in Table II. Systematic uncertainties originate from (i) parameter choices of the analysis procedures and (ii) possible differences in the locations and energy spectra between the calibration sources and background events. The combined errors of $\mathrm{AC}^- \otimes \mathrm{B}_0$ are dominated by the statistical uncertainties in the measurement of (B,S), boosted by the factor of $[1/(\epsilon_{\rm BS}+\lambda_{\rm BS}-1)]$ from Eq. (2) as $(\epsilon_{\rm BS}, \lambda_{\rm BS})$ deviates from unity below 1.5 keVee. Contributions of systematic uncertainties are minor (increasing the total error of $\mathrm{AC}^- \otimes \mathrm{B}_0$ from 1.47 to 1.71 $\mathrm{kg}^{-1}\,\mathrm{keVee}^{-1}\,\mathrm{day}^{-1}$ at threshold) and are taken into account in the analysis. The variations of the key parameters over changes of τ_0 within the τ-scan range in Fig. 1(a)

TABLE I. The various contributions to the total error of $AC^- \otimes B_0$ at threshold and at a typical high energy bin.

Energy bin	0.475–0.575 keVee	1.975–2.075 keVee
$AC^- \otimes B_0$ and errors (kg^{-1} $keVee^{-1}$ day^{-1})	$4.09 \pm 1.47[\text{stat}] \pm 0.87[\text{sys}] = 4.09 \pm 1.71$	$4.22 \pm 0.97[\text{stat}] \pm 0.27[\text{sys}] = 4.22 \pm 1.01$
(I) Statistical uncertainties (combined):	1.47	0.97
(i) Uncertainties on calibration $(\epsilon_{BS}, \lambda_{BS})$:	0.32	0.08
(ii) Derivation of $(\epsilon_{BS}, \lambda_{BS})$-corrected bulk rates:	1.43	0.97
(II) Systematic uncertainties (combined):	0.87	0.27
(i) Rise-time cut value τ_0	0.27	0.12
(ii) Fiducial mass	0.05	0.05
(iii) Normalization range (3–5 keVee)	0.07	0.01
(iv) $(B_0, S_0) = (B, S)$ at normalization	0.10	0.10
(v) Choice of discard region	0.30	0.06
(vi) Source location	0.28	0.19
(vii) Source energy range and spectra	0.72	0.12

are studied. The B_0 spectra are stable, robust and independent of τ_0, as indicated by the small variations relative to the uncertainties.

The high statistics of ^{241}Am surface events produce the narrow vertical bands in Fig. 2(b), which in turn drives the small statistical error of λ_{BS} in Fig. 2(c). An additional stress test was performed. The ^{241}Am measurements are discarded altogether, and $(\epsilon_{BS}, \lambda_{BS})$ are derived with the ^{57}Co, ^{137}Cs and ^{60}Co data. The results are summarized in Table II. The B_0 at the threshold energy bin would be shifted only by 4.2% from 4.09 to 3.92 kg^{-1} $keVee^{-1}$ day^{-1}. The effects on the subsequent physics analysis are therefore negligible.

High energy γ rays from ambient radioactivity produce flat electron-recoil background at low energy, as predicted by simulations and is verified by the ^{241}Am, ^{137}Cs and ^{60}Co spectra of Fig. 2(a). The L-shell x-ray lines are predicted by the K-shell peaks. Both background are subtracted from the $(\epsilon_{BS}, \lambda_{BS})$-corrected $AC^- \otimes B_0$ spectrum as shown in Fig. 3(b). A minimum-χ^2 analysis is applied to the residual spectrum within 0.475 and 2.25 keVee, adopting two free and positive definite parameters which characterize the flat ambient γ background and the possible χ-N spin-independent cross section ($\sigma^{SI}_{\chi N}$), respectively. Conventional astrophysical models [1] are adopted to describe WIMP-induced interactions, using the local WIMP density of 0.3 GeV/cm^3, the Maxwellian velocity distribution with $v_0 = 220$ km/s and the galactic escape velocity of $v_{esc} = 544$ km/s. The quenching function (QF) in Ge is evaluated with the TRIM software package [23]. The derived QF is depicted in Fig. 4 with measured data [24] showing good agreement over a large range of nuclear recoil energy. A systematic uncertainty of 10% is taken, corresponding to the spread of individual data points, as well as the deviations with the alternative Lindhard model [25]. Analysis is performed by scanning QF within $\pm 10\%$ of their nominal value, and the most conservative constraints are adopted as the limits.

As illustration, the best-fit spectrum at $m_\chi = 8$ GeV, where $\sigma^{SI}_{\chi N} = (-1.80 \pm 9.28) \times 10^{-42}$ cm^2 at $\chi^2/\text{d.o.f} = 8.11/16$ (p-value $= 0.95$), is depicted in Fig. 3(b), with the band representing the 2σ uncertainties. Exclusion plot of $\sigma^{SI}_{\chi N}$ versus m_χ at 90% confidence level is displayed in Fig. 5. The bounds from other benchmark experiments are superimposed [3,7,9,10]. As comparison, different QFs (parametrization of CoGeNT [3] and Lindhard theory with

TABLE II. Uncertainty values of $(\epsilon_{BS}, \lambda_{BS})$ and B_0 at the most important threshold energy bin. While systematic errors are important to the $(\epsilon_{BS}, \lambda_{BS})$ measurements, the dominant contributions to the uncertainties in the physics rate B_0 remain those from statistical errors due to limited counts. Discarding the statistically strong ^{241}Am measurements in a stress test would not introduce significant changes to B_0, on which subsequent physics analysis are based.

Threshold bin (475–575) eVee	ϵ_{BS} [$\pm\Delta$]	λ_{BS} [$\pm\Delta$]	B_0 [$\pm\Delta$] (kg^{-1} keV^{-1} day^{-1})
Reference analysis	$0.757 \pm 0.051(6.7\%)$ [stat] $\pm 0.112(14.8\%)$ [sys] $= 0.757 \pm 0.123(16.2\%)$ [total]	$0.882 \pm 0.001(0.1\%)$ [stat] $\pm 0.020(2.0\%)$ [sys] $= 0.882 \pm 0.020(2.0\%)$ [total]	$4.09 \pm 1.47(35.9\%)$ [stat] $\pm 0.87(21.3\%)$ [sys] $= 4.09 \pm 1.71(41.8\%)$ [total]
Stress test (Discard ^{241}Am data)	$0.673 \pm 0.074(11.0\%)$ [stat] $\pm 0.112(16.6\%)$ [sys] $= 0.673 \pm 0.134(20.0\%)$ [total]	$0.862 \pm 0.007(0.8\%)$ [stat] $\pm 0.020(2.3\%)$ [sys] $= 0.862 \pm 0.021(2.4\%)$ [total]	$3.92 \pm 1.53(39.0\%)$ [stat] $\pm 0.91(23.2\%)$ [sys] $= 3.92 \pm 1.78(45.4\%)$ [total]

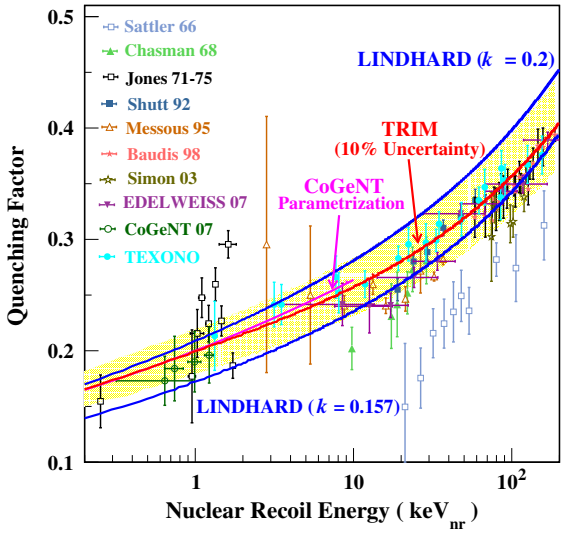

FIG. 4 (color online). The QF curve which is derived from TRIM [23] as a function of nuclear recoil energy, together with a ±10% band (light shadow band). The various experimental measurements are overlaid, so are the alternative QFs from parametrization of CoGeNT [3] and the Lindhard theory [25] at $k = 0.2$ and $k = 0.157$ adopted by CDMSlite [9]. It can be see that the TRIM results with uncertainties covers most data points as well as the alternative formulations.

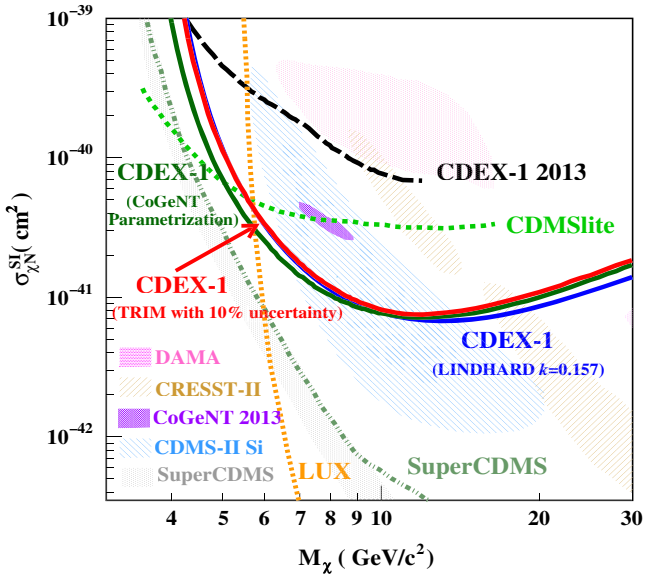

FIG. 5 (color online). The 90% confidence level upper limit of spin-independent χN coupling. The CDEX-1 results from this work are depicted in solid red. Bounds from alternative QF formulations are represented as solid blue and green curves. Results from other benchmark experiments [2–5,7,9,10,14] are superimposed.

$k = 0.157$ of CDMSlite [9]) are used to derive alternative exclusion curves, also displayed in Fig. 5. It can be seen that the analysis procedures adopted in this work provide the most conservative constraints.

An order of magnitude improvement in the sensitivities of $\sigma^{\mathrm{SI}}_{\chi\mathrm{N}}$ has been achieved over our previous results [14]. Part of the light WIMP regions within 6 and 20 GeV implied by earlier experiments are probed and rejected. In particular, the CoGeNT anomalous events at sub-keV energy [3] are not reproduced in these results based on identical detector techniques. This strongly disfavors that the excess is induced by dark matter, independent of interaction channels. For instance, electromagnetic final states are not constrained by experiments like SuperCDMS [10] which measure nuclear recoil events. They can, however, be probed by the CDEX-1 data.

The CDEX-1 experiment continues to accumulate data at CJPL. Research programs are pursued to further reduce the physics threshold via hardware and software efforts. Time modulation of the data will be studied. A *p*PCGe array of 10 kg target mass range enclosed in an active liquid argon anti-Compton detector is being constructed. Feasibility studies towards scale-up to ton-scale experiment [20] are being pursued.

This work was supported by the National Natural Science Foundation of China (Contracts No. 10935005, No. 10945002, No. 11275107, No. 11175099) and National Basic Research program of China (973 Program) (Contract No. 2010CB833006) and NSC 99-2112-M-001-017-MY3 and Academia Sinica Principal Investigator 2011-2015 Grant from Taiwan.

[1] M. Drees and G. Gerbier, Phys. Rev. D **88**, 012002 (2013), and references therein.
[2] R. Bernabei *et al.*, Eur. Phys. J. C **56**, 333 (2008); **67**, 39 (2010).
[3] C. E. Aalseth *et al.*, Phys. Rev. D **88**, 012002 (2013); arXiv:1401.3295.
[4] G. Angloher *et al.*, Eur. Phys. J. C **72**, 1971 (2012).
[5] R. Agnese *et al.*, Phys. Rev. Lett. **111**, 251301 (2013).
[6] E. Aprile *et al.*, Phys. Rev. Lett. **109**, 181301 (2012).
[7] D. S. Akerib *et al.*, Phys. Rev. Lett. **112**, 091303 (2014).
[8] H. B. Li *et al.*, Phys. Rev. Lett. **110**, 261301 (2013).
[9] R. Agnese *et al.*, Phys. Rev. Lett. **112**, 041302 (2014).
[10] R. Agnese *et al.*, Phys. Rev. Lett. **112**, 241302 (2014).
[11] Q. Yue *et al.*, High Energy Phys. Nucl. Phys. **28**, 877 (2004); H. T. Wong, H. B. Li, J. Li, Q. Yue, and Z. Y. Zhou, J. Phys. Conf. Ser. **39**, 266 (2006).

[12] P. N. Luke, F. S. Goulding, N. W. Madden, and R. H. Pehl, IEEE Trans. Nucl. Sci. **36**, 926 (1989); P. A. Barbeau, J. I. Collar, and O. Tench, J. Cosmol. Astropart. Phys. 09 (2007) 009.
[13] H. T. Wong, Mod. Phys. Lett. A **23**, 1431 (2008); S. T. Lin *et al.*, Phys. Rev. D **79**, 061101 (2009).
[14] W. Zhao *et al.*, Phys. Rev. D **88**, 052004 (2013); K. J. Kang *et al.*, Chin. Phys. C **37**, 126002 (2013).
[15] G. K. Giovanetti *et al.*, Phys. Procedia **00**, 1 (2014).
[16] K. J. Kang, J. P. Cheng, Y. H. Chen, Y. J. Li, M. B. Shen, S. Y. Wu, and Q. Yue, J. Phys. Conf. Ser. **203**, 012028 (2010).
[17] Y. C. Wu *et al.*, Chin. Phys. C **37**, 086001 (2013).
[18] S. K. Liu *et al.*, Phys. Rev. D **90**, 032003 (2014).
[19] H. B. Li *et al.*, Astropart. Phys. **56**, 1 (2014).
[20] K. J. Kang *et al.*, Front. Phys. **8**, 412 (2013).
[21] U. Tamm, W. Michaelis, and P. Coussieu, Nucl. Instrum. Methods **48**, 301 (1967); M. G. Strauss and R. N. Larsen, Nucl. Instrum. Methods **56**, 80 (1967); E. Sakai, IEEE Trans. Nucl. Sci. **18**, 208 (1971).
[22] E. Aguayo *et al.*, Nucl. Instrum. Methods Phys. Res., Sect. A **701**, 176 (2013).
[23] J. F. Ziegler, http://www.srim.org.
[24] S. T. Lin *et al.*, arXiv:0712.1645v4, and references therein.
[25] J. Lindhard *et al.*, K. Dan. Vidensk. Selsk. Mat. Fys. Medd. **33**, 10 (1963).